Cell Death and Differentiation (2017), 1079–1090
 1350-9047/17

www.nature.com/cdd

Phospholipase Cδ1 regulates p38 MAPK activity and skin barrier integrity

Kaori Kanemaru[1,7], Yoshikazu Nakamura*[,1,2,7], Kengo Totoki[1], Takatsugu Fukuyama[1], Madoka Shoji[1], Hisae Kaneko[1], Kanako Shiratori[1], Atsuko Yoneda[1,3], Takafumi Inoue[4], Yoichiro Iwakura[5], Kenji Kabashima[6] and Kiyoko Fukami*[,1,3]

Keratinocytes undergo a unique type of programmed cell death known as cornification, which leads to the formation of the stratum corneum (SC), the main physical barrier of the epidermis. A defective epidermal barrier is a hallmark of the two most common inflammatory skin disorders, psoriasis, and atopic dermatitis. However, the detailed molecular mechanisms of skin barrier formation are not yet fully understood. Here, we showed that downregulation of phospholipase C (PLC) δ1, a Ca^{2+}-mobilizing and phosphoinositide-metabolizing enzyme abundantly expressed in the epidermis, impairs the barrier functions of the SC. PLCδ1 downregulation also impairs localization of tight junction proteins. Loss of PLCδ1 leads to a decrease in intracellular Ca^{2+} concentrations and nuclear factor of activated T cells activity, along with hyperactivation of p38 mitogen-activated protein kinase (MAPK) and inactivation of RhoA. Treatment with a p38 MAPK inhibitor reverses the barrier defects caused by PLCδ1 downregulation. Interestingly, this treatment also attenuates psoriasis-like skin inflammation in imiquimod-treated mice. These findings demonstrate that PLCδ1 is essential for epidermal barrier integrity. This study also suggests a possible link between PLCδ1 downregulation, p38 MAPK hyperactivation, and barrier defects in psoriasis-like skin inflammation.
Cell Death and Differentiation (2017) **24,** 1079–1090; doi:10.1038/cdd.2017.56; published online 21 April 2017

The skin is a barrier organ in which keratinocytes defend the organism against the external environment. Keratinocytes undergo a unique type of programmed cell death known as cornification, which leads to the formation of the stratum corneum (SC), the main physical barrier.[1,2] Tight junctions (TJs) also contribute to barrier function by sealing the intercellular spaces in the stratum granulosum (SG).

Disruption of skin barrier is the primary cause of atopic dermatitis (AD).[3,4] Barrier function is also altered in psoriasis.[5,6] Recent identification of epidermal genes as psoriasis risk factors suggests that barrier abnormalities underlie the pathogenesis of psoriasis.[7,8] However, the molecular mechanisms of barrier disturbance in psoriasis have not yet been fully clarified.

Adequate elevation of the intracellular Ca^{2+} concentration ($[Ca^{2+}]_i$) has a critical role in TJ and SC barrier formations.[9] Besides $[Ca^{2+}]_i$ elevation, phosphoinositide metabolism also has a critical role in the terminal differentiation of keratinocytes.[10–12] Phospholipase C (PLC) regulates both $[Ca^{2+}]_i$ elevation and phosphoinositide metabolism. One of the PLC isozymes, PLCδ1, is abundantly expressed in the SG and is downregulated in the lesional skin of patients with psoriasis.[13] However, it is not clear whether PLCδ1 downregulation contributes to a defective epidermal barrier, a hallmark of psoriasis.

The present study reveals that a loss of epidermal PLCδ1 impairs epidermal barrier function through dysregulation of Ca^{2+} and p38 mitogen-activated protein kinase (MAPK) signaling. This study also reveals a possible link among PLCδ1 downregulation, p38 MAPK hyperactivation, and barrier defects in psoriasis-like skin inflammation.

Results

Epidermal loss of PLCδ1 impairs barrier function. Since a defective skin barrier is a characteristic feature of psoriasis, we examined the contribution of PLCδ1 downregulation to skin barrier defects. To this end, skin permeability to fluorescein isothiocyanate (FITC) was evaluated. FITC signals were barely detected in the SC of 6-month-old control mice, whereas FITC penetrated and accumulated in the SC of the 6-month-old PLCδ1 knockout (KO) mice (Figure 1a). Quantification analyses with a fluorometer revealed that the epidermis of PLCδ1 KO mice contained a higher amount of FITC than the epidermis of control mice (Figure 1b). Increased FITC accumulation was also observed in younger, 2-month-old PLCδ1 KO mice (mean $\pm$ standard error of mean (S.E.M.), 5.5 ± 0.37 ng/cm^2 in control mice *versus* 11 ± 0.041 ng/cm^2 in PLCδ1 KO mice; $N=4$ in each group; $P<0.01$). These results indicate that the outside–inside barrier function against FITC is impaired in PLCδ1 KO skin. In contrast, transepidermal water loss was not increased in PLCδ1 KO mice (Supplementary Figure S1). We next examined the effects of PLCδ1 downregulation on the SC. The cornified

[1]Laboratory of Genome and Biosignals, School of Life Sciences, Tokyo University of Pharmacy and Life Sciences, Tokyo, Japan; [2]PRIME, Japan Agency for Medical Research and Development, Tokyo, Japan; [3]AMED-CREST, Japan Agency for Medical Research and Development, Tokyo, Japan; [4]Department of Life Science and Medical Bioscience, Waseda University, Tokyo, Japan; [5]Center for Animal Disease Models, Research Institute for Biomedical Sciences, Tokyo University of Science, Chiba, Japan and [6]Department of Dermatology, Kyoto University Graduate School of Medicine, Kyoto, Japan

*Corresponding author: Y Nakamura or K Fukami, Laboratory of Genome and Biosignals, School of Life Sciences, Tokyo University of Pharmacy and Life Sciences, 1432-1 Horinouchi, Hachioji, Tokyo, Japan. Tel: 81-42-676-7232; Fax: 81-42-676-7249; E-mail: ynakamur@toyaku.ac.jp or kfukami@toyaku.ac.jp

[7]These authors contributed equally to this work.

Received 03.9.16; revised 09.3.17; accepted 14.3.17; Edited by RA Knight; published online 21.4.2017

envelopes (CEs) from PLCδ1 KO skin were smaller and irregularly round in shape compared to those from the control (Figure 1c). In addition, CEs from PLCδ1 KO skin were more susceptible to mechanical stress (Figure 1c). The degradation slope of linear trendline is significantly steeper in PLCδ1 KO samples than that in control samples (mean ± S.E.M. Slopes, −5.4 ± 0.56 in controls *versus* −7.3 ± 0.25 in PLCδ1 KO mice, both $N=4$. $P<0.05$.). These observations suggest that CEs maturation is impaired in PLCδ1 KO skin. The number of CEs was higher in PLCδ1 KO skin (Figure 1c), which was probably caused by the thickened SC (Figure 1d, upper panels). CE maturation is important for lipid matrix formation in the SC.[14] Consistent with the observation of immature CEs, Nile red staining of lipids was very low in the SC of PLCδ1 KO mice (Figure 1e). As lipid matrix in the SC is important in skin barrier function, abnormal formation of lipid matrix may contribute to barrier defects in PLCδ1 KO skin. Further, transmission electron microscopy revealed that the SC of PLCδ1 KO mice was swollen and contained aberrant filamentous aggregates, which was not observed in the control SC (Figure 1d, lower panels). Filaggrin—a protein critical for the SC barrier—is degraded in the SC by proteases to generate important components of SC barrier function, such as a natural moisturizing factor. Filaggrin staining was confined to the lower SC in control mice, whereas the SC of PLCδ1 KO mice exhibited broad filaggrin

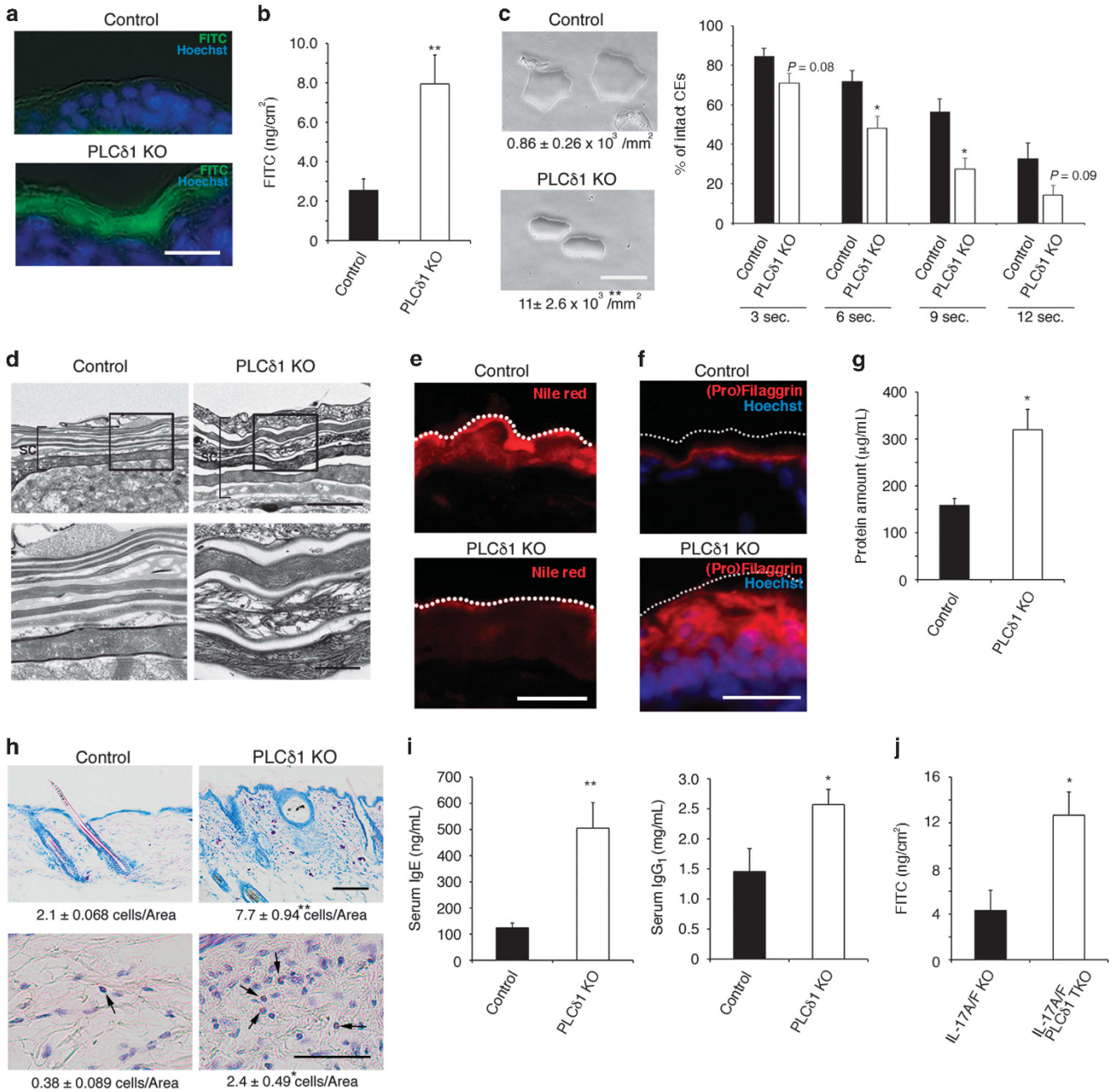

staining, where the upper SC also stained positive (Figure 1f), suggesting that filaggrin degradation is impaired in the SC of PLCδ1 KO mice. Further, tape stripping removed approximately twofold more protein from the SC of PLCδ1 KO mice than from the SC of control mice (Figure 1g), suggesting that the SC of PLCδ1 KO mice is more fragile and unstable. PLCδ1 KO mice also showed increased numbers of mast cells and eosinophils in the dermis (Figure 1h) and elevated serum IgE and IgG_1 (Figure 1i). This is characteristic of mild allergic inflammation and represents a typical immune response to skin barrier defects. The skin of PLCδ1 KO mice shows increased levels of IL-17.[13] As IL-17 decreases barrier proteins,[15] loss of PLCδ1 might disturb the skin barrier through IL-17 overproduction. However, loss of IL-17A/F did not restore the normal skin barrier in PLCδ1 KO skin (Figure 1j). Transgenic reintroduction of the *PLCδ1* gene into the keratinocytes of PLCδ1 KO mice (Tg/KO) restored normal barrier permeability against FITC (Supplementary Figure S2a). Moreover, the SC of these mice showed normal lipid staining (Supplementary Figure S2b), as well as a normal number of regularly shaped CEs (Supplementary Figure S2c). On the other hand, keratinocyte-specific PLCδ1 KO (cKO) mice presented defects in the barrier functions, SC lipids, and CEs (Supplementary Figures S2d–f). These results indicate that epidermal loss of PLCδ1 is responsible for the defective epidermal barrier. Loss of PLCδ1 did not disturb expression of epidermal differentiation markers such as K1, loricrin and involucrin[13] and transglutaminase activity in SC (Supplementary Figures S3a and b). On the other hand, aberrant suprabasal expression of K5 was observed in PLCδ1 cKO epidermis, which is probably caused by skin inflammation (Supplementary Figure S3a). PLCδ1 cKO newborn mice did not show obvious defects in the structure of the epidermis, expression of differentiation and proliferation markers, or CEs formation (Supplementary Figures S4a, b and f). Toluidine blue penetration was not increased in PLCδ1 cKO newborn mice (Supplementary Figure S4c), whereas increased penetration of toluidine blue and lucifer yellow was observed in ventral skin as early as P8 (Supplementary Figures S4d and e), suggesting that PLCδ1 is dispensable for SC barrier formation in newborn mice, but is required for SC barrier maintenance after P8.

PLCδ1 downregulation impairs skin barrier function through inflammatory immune cells-independent mechanisms. Inflammatory cytokines from immune cells impair skin barrier integrity.[16,17] As epidermal loss of PLCδ1 results in immune cell infiltration and cytokine overproduction in the skin[13,18] and skin barrier defects were observed at the same timing of onset of immune cell infiltration[18] (Supplementary Figures S4d and e), skin barrier defects might be a secondary effect of immune cell infiltration. Therefore, we took advantage of a human organotypic skin culture system, which consists of human dermal fibroblasts and epidermal keratinocytes. We generated human organotypic skin cultures of normal human epidermal keratinocytes (NHEK) with either a non-targeting or *PLCδ1*-targeting siRNA (Figures 2a and b). Then, we evaluated the permeability barrier by the lucifer yellow penetration assay. Lucifer yellow penetrated and accumulated in the SC and upper epidermis of the PLCδ1-knocked down skin culture, but not in those of the control culture (Figure 2c). Filaggrin showed a broad expression pattern in the SC of PLCδ1-knocked down skin culture (Figure 2d). Interestingly, active caspase-14, a critical enzyme for filaggrin degradation and skin barrier formation,[19,20] was decreased in the PLCδ1-knocked down skin culture (Figure 2e). PLCδ1 downregulation did not disturb thickness of epidermis and expression of the differentiation marker involucrin and the proliferation marker Ki67 (Supplementary Figure S5a), suggesting that PLCδ1 downregulation does not affect general differentiation and proliferation of keratinocytes in the organotypic skin culture. Thus, PLCδ1 downregulation disturbs barrier integrity in a human organotypic skin culture system through inflammatory immune cell-independent mechanisms.

***PLCδ1* silencing inhibits TJ formation in human keratinocytes.** TJ functions as a barrier by sealing the intercellular spaces in the SG. As PLCδ1 is abundantly expressed in the SG,[13] we examined whether *PLCδ1* silencing affects TJ. Immunofluorescence revealed that *PLCδ1* silencing

Figure 1 PLCδ1 KO mice exhibit defective barrier permeability. (**a**) After topical application of FITC (green), fluorescence was visualized in dorsal skin sections of control and PLCδ1 KO mice. Nuclei were counter-stained with Hoechst (blue). Scale bar = 20 μm. ($N = 4$ in each group). Images are representative of four animals per group. Stained sections were assessed in a blinded fashion by two independent observers. (**b**) FITC intensity was measured in dorsal skin lysates from control and PLCδ1 KO mice. Data are represented as mean ± S.E.M. ($N = 4$ in each group). (**c**) Representative micrographs of CEs from control and PLCδ1 KO dorsal skin. Numbers of CEs are also shown (CEs/mm^2). The percentages of intact CEs after sonication for indicated time are also shown. Data are represented as mean ± S.E.M. ($N = 4$ in each group). Scale bar = 50 μm. (**d**) Transmission electron microscope (T.E.M) analysis of SC. A magnified view of the indicated area (square in upper panels) is shown in the lower panels. Scale bar = 2 μm (upper panels), and 0.5 μm (lower panels). Images are representative of two animals per group and were assessed in a blinded fashion by two independent observers. (**e**) Nile red staining of control and PLCδ1 KO dorsal skin sections. Dotted lines denote the skin surface. Scale bar = 30 μm. Images are representative of three animals per group. Stained sections were assessed in a blinded fashion by two independent observers. (**f**) Dorsal skin sections of control and PLCδ1 KO mice were stained with an antibody against (pro) filaggrin (red). Nuclei were counter-stained with Hoechst (blue). Dotted lines denote the skin surface. Scale bar = 50 μm. Images are representative of three animals per group. Stained sections were assessed in a blinded fashion by two independent observers. (**g**) Quantification of the protein removed by tape stripping (25 μL/cm^2). Data are represented as mean ± S.E.M. ($N = 3$ in each group). (**h**) Mast cells (upper panels) and eosinophils (lower panels) were stained with toluidine blue and Congo red, respectively, in control and PLCδ1 KO dorsal skin sections. Arrows in lower panels indicate Congo red-positive cells. Numbers of mast cells and eosinophils are also shown. Data are represented as mean ± S.E.M. ($N = 4$ in each group). Scale bar = 100 μm (upper panels), and 50 μm (lower panels). (**i**) Serum IgE and IgG_1 concentrations in control and PLCδ1 KO mice. Data are represented as mean ± S.E.M. ($N = 7$ in each group). (**j**) A FITC penetration assay was performed with IL-17A/F KO and IL-17A/F, PLCδ1 triple KO (IL-17A/F PLCδ1 TKO) mice. FITC intensity was measured in skin lysates. Data are represented as mean ± S.E.M. ($N = 4$ in each group). Six-month-old mice (**a** and **b**) and two to three-month old mice (**c**–**j**) were used. Statistical significance was assessed using Welch's *t*-test. $^*P < 0.05$, $^{**}P < 0.01$

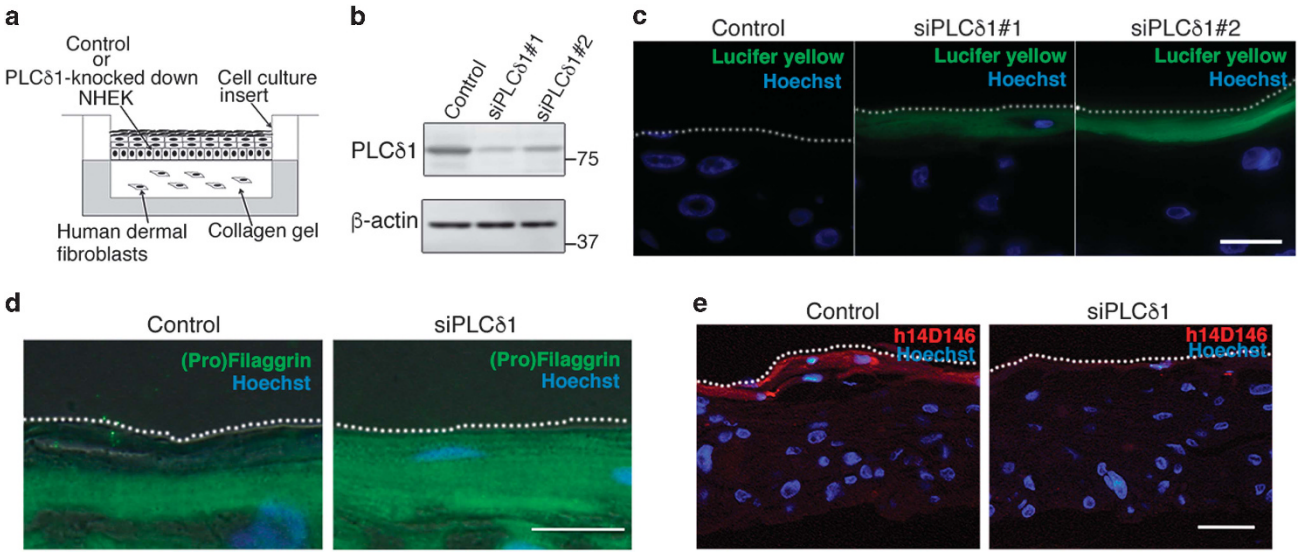

Figure 2 *PLCδ1* silencing impairs the epidermal barrier in human organotypic skin culture. (**a**) Schematic representation of an organotypic skin culture. (**b**) Immunoblotting for PLCδ1 in a human organotypic skin culture. Either non- (control) or *PLCδ1*-targeting siRNAs (siPLCδ1#1 and siPLCδ1#2) were introduced into NHEK. β-actin was used as a loading control. Results are representative of three trials. (**c**) Lucifer yellow fluorescence (green) was visualized in sections of NHEK organotypic skin cultures treated with either non- (control) or *PLCδ1*-targeting (siPLCδ1#1 and siPLCδ1#2) siRNAs. Nuclei were counter-stained with Hoechst (blue). Dotted lines denote the skin culture surface. Scale bar = 30 μm. Images are representative of four trials. Stained sections were assessed in a blinded fashion by two independent observers. (**d**, **e**) Immunofluorescence detection of (pro)filaggrin (green) (**d**) and active caspase-14 (h14D146; red) (**e**) in sections of NHEK organotypic skin cultures treated with either non- (control) or *PLCδ1*-targeting (siPLCδ1) siRNAs. Nuclei were counter-stained with Hoechst (blue). Dotted lines denote the skin culture surface. Scale bar = 20 μm (**d**) and 50 μm (**e**). Images are representative of three trials. Stained sections were assessed in a blinded fashion by two independent observers

diminished staining of the TJ protein ZO-1 in NHEK (Figure 3a). *PLCδ1* silencing also disturbed localization of other TJ proteins such as claudin-1 and occludin (Supplementary Figure S6a). In contrast, staining of E-cadherin was largely unaffected (Figure 3a). *PLCδ1* silencing did not alter the amount of ZO-1 protein (Figure 3b), indicating that PLCδ1 downregulation impairs the membrane localization of ZO-1. PLCδ1 knockdown also decreased transepithelial electrical resistance (TEER), a functional parameter of TJ barrier permeability, in NHEK compared to the TEER in NHEK transfected with a non-targeting siRNA control (Table 1). In addition, staining of ZO-1 and claudin-1 was weak in PLCδ1-knocked down organotypic skin culture (Figure 3c; Supplementary Figure S6b). TEER was also decreased by PLCδ1 downregulation (Supplementary Table S1), suggesting that TJ or SC barrier are impaired in PLCδ1-knockdown organotypic skin cultures. We further examined infiltration of biotin tracers to assess functions of TJ in PLCδ1-knockdown organotypic skin cultures. Although PLCδ1-knocked down organotypic skin culture showed stronger biotin tracer signal in the upper SG, tracer was stopped at the top of the SG, suggesting that PLCδ1 downregulation did not abolish TJ barrier against biotin tracer and that decreased TEER in PLCδ1-knocked down organotypic skin culture is mainly caused by impaired SC barrier (Supplementary Figure S5b). Consistent with the *in vitro* results, ZO-1 showed faint staining in the PLCδ1 cKO epidermis (Figure 3d). Although claudin-1 expression was not obviously altered in PLCδ1 cKO epidermis, occludin staining was diffuse and faint in the PLCδ1 cKO epidermis (Supplementary Figure S6c). Collectively, these data indicate that reduced expression of PLCδ1 disturbs localization of TJ proteins. Next, we performed a Rho-binding domain (RBD) pull-down assay to examine the effect of PLCδ1 knockdown on RhoA-GTP, a regulator of TJ formation.[21] The results showed that *PLCδ1* silencing decreased RhoA-GTP levels (Figure 3e) in NHEK upon Ca^{2+} stimulation. This reduction was also confirmed by G-LISA (Figure 3f). The amount of another regulator of TJ formation, Rac1-GTP, was not altered by PLCδ1 knockdown (Supplementary Figure S7). Interestingly, the addition of the RhoA activator CNFy partially restored ZO-1 membrane localization in PLCδ1-knocked down NHEK (Figure 3g), suggesting that insufficient RhoA activation contributes to defective TJ formation in PLCδ1-knocked down NHEK.

PLCδ1 downregulation impairs $[Ca^{2+}]_i$ elevation and NFAT activation. We next examined whether PLCδ1 downregulation affects $[Ca^{2+}]_i$ mobilization in NHEK. *PLCδ1* silencing inhibited $[Ca^{2+}]_i$ elevation in response to Ca_o^{2+} in NHEK (Figure 4a). On the other hand, ATP-induced $[Ca^{2+}]_i$ elevation was observed in PLCδ1-knocked down NHEK, suggesting that impaired Ca_o^{2+}-induced elevation of $[Ca^{2+}]_i$ in PLCδ1-knocked down NHEK was not due to decreased viability of cells (Supplementary Figure S8a). The store-operated Ca^{2+} channel (SOC) activity was not impaired by PLCδ1 knockdown (Figure 4b), suggesting that the defect in $[Ca^{2+}]_i$ elevation in PLCδ1-knocked down NHEK is due to impaired Ca^{2+} release from intracellular stores. $[Ca^{2+}]_i$ elevation induces nuclear translocation of the transcription factor NFAT, which induces the expression of NFAT-responsive genes. As keratinocytes express all four NFAT family members (NFATc1 to c4)[22,23] and subcellular

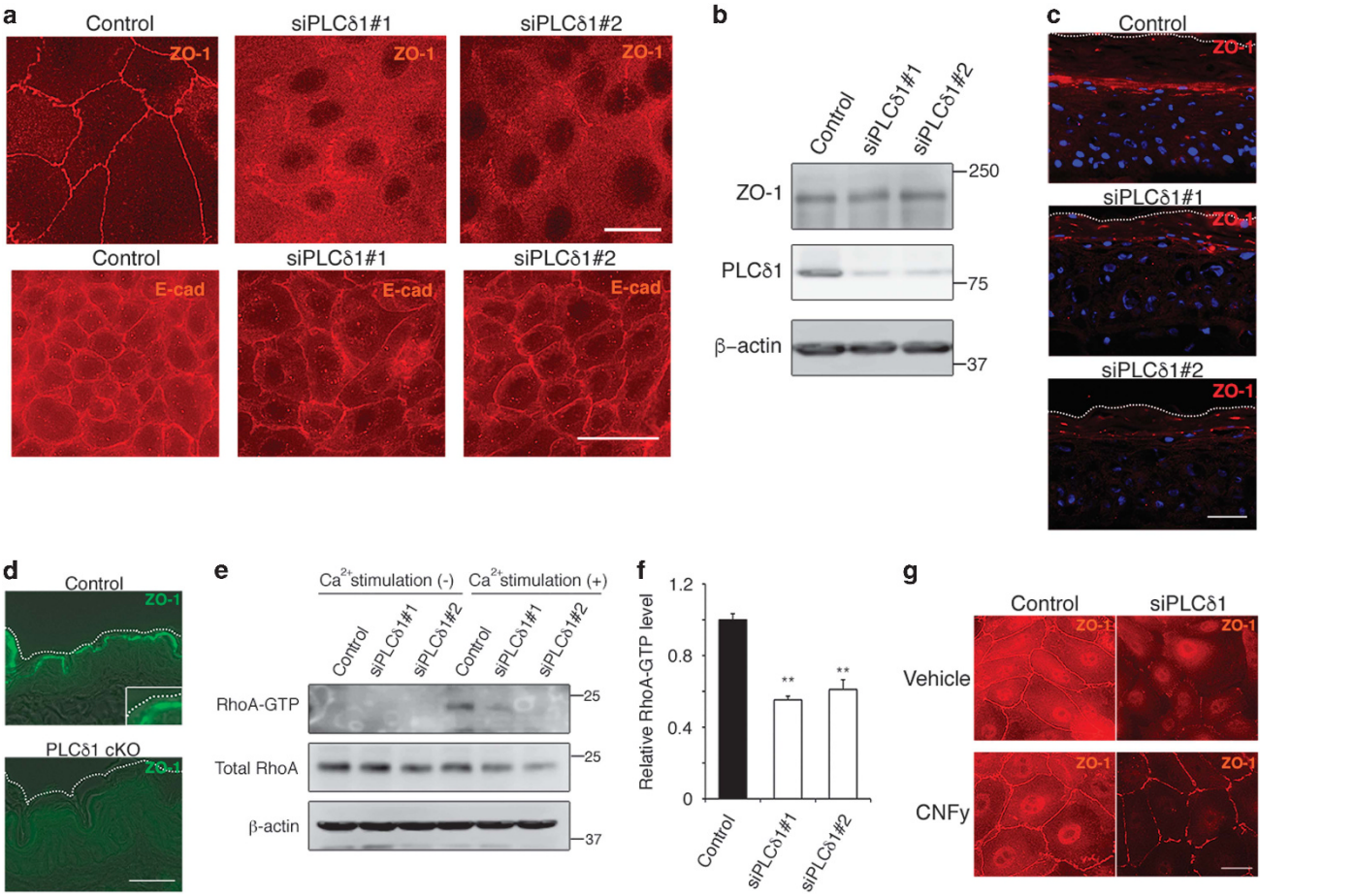

Figure 3 *PLCδ1* silencing inhibits TJ formation and RhoA activation in NHEK. (**a**) NHEK treated with either non- (control) or *PLCδ1*-targeting (siPLCδ1#1 and siPLCδ1#2) siRNAs were stained for ZO-1 (upper panels) and E-cadherin (E-cad, lower panels) after 24 h of incubation with medium containing 1.2 mM $CaCl_2$. Scale bar = 50 μm (upper panels) and 100 μm (lower panels). Images are representative of three trials. (**b**) Immunoblotting for ZO-1 and PLCδ1 in NHEK grown in medium containing 1.2 mM $CaCl_2$ for 24 h. β-actin was used as a loading control. Results are representative of three trials. (**c**) Immunofluorescence detection for ZO-1 in sections of NHEK organotypic skin cultures treated with either non- (control) or *PLCδ1*-targeting (siPLCδ1#1, siPLCδ1#2) siRNAs. Nuclei were counter-stained with Hoechst (blue). Dotted lines denote the skin culture surface. Scale bar = 20 μm. (**d**) Skin samples of control and keratinocyte-specific PLCδ1 knockout (cKO) mice were stained with an antibody against ZO-1. Dotted lines denote the surface of the skin. Scale bar = 20 μm. Insert: higher magnification of the border between granular layer and SC. Images are representative of three animals per group. Stained sections were assessed in a blinded fashion by two independent observers. (**e**) NHEK treated with either non- (control) or *PLCδ1*-targeting (siPLCδ1#1 and siPLCδ1#2) siRNAs were exposed to 2 mM $CaCl_2$ for 15 min (Ca^{2+} stimulation). Activated RhoA (RhoA-GTP) was analyzed by immunoblotting using a glutathione-*S*-transferase-rho-binding domain (GST-RBD) pull-down. Total RhoA and β-actin in whole cell lysates were also examined. Results are representative of three trials. (**f**) The RhoA-GTP levels were determined using G-LISA in NHEK stimulated with Ca^{2+}. The RhoA-GTP levels were normalized to the total protein amount. Data are represented as mean ± S.E.M. (N = 3 in each group). (**g**) Immunofluorescence detection of ZO-1 in NHEK treated with either non- (control) or *PLCδ1*-targeting (siPLCδ1) siRNAs grown in medium containing 1.2 mM $CaCl_2$ and treated with either vehicle or a RhoA activator (CNFy). Scale bar = 30 μm. Images are representative of three trials. Statistical significance was assessed using Welch's *t*-test. $^{**}P < 0.01$

Table 1 TEER of normal NHEK treated with either non- (control) or *PLCδ1*-targeting siRNAs

	Vehicle			20 μM SB202190	
	Control	**siPLCδ1#1**	**siPLCδ1#2**	**siPLCδ1#1**	**siPLCδ1#2**
TEER (Ω cm^2)	300 ± 11	120 ± 0.18**	150 ± 8**	210 ± 7.5**	300 ± 13

$^{**}P < 0.01$ vs. control
Mean ± S.E.M. (N = 3 in each group). Welch's *t*-test

(cytoplasmic *versus* nuclear) localization is similarly regulated,[24] we examined localization of an NFAT family member, NFATc4. *PLCδ1* silencing decreased the nuclear translocation of NFATc4 (Figure 4c) without affecting the amount of NFATc4 protein (Supplementary Figure S8b). In addition, *PLCδ1* silencing inhibited NFAT-responsive reporter activity under high $CaCl_2$ conditions in NHEK (Figure 4d). Treatment of NHEK with the NFAT inhibitor 11R-VIVIT decreased TEER (Table 2) without affecting the amount of TJ proteins such as ZO-1 and claudin-1 (Supplementary

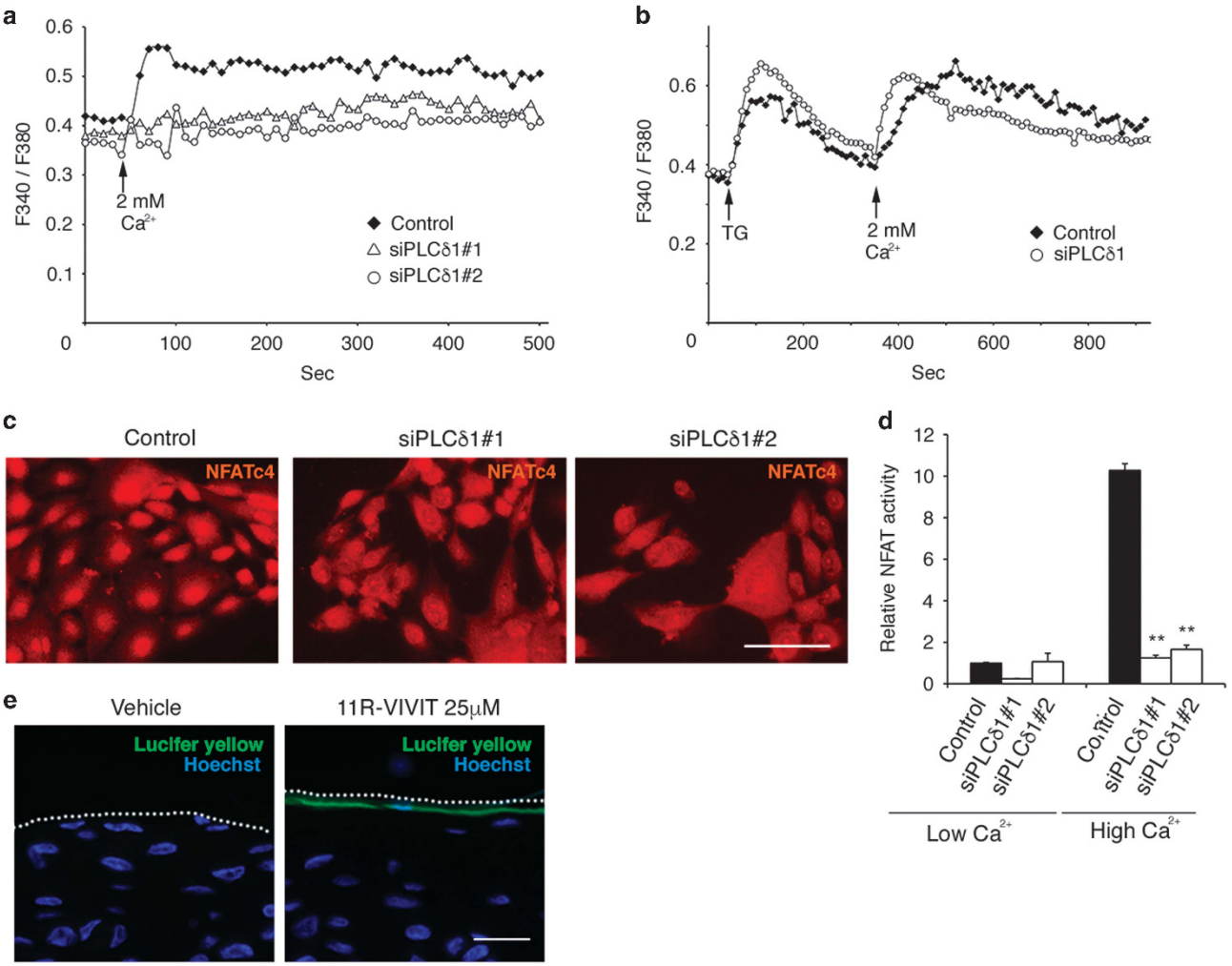

Figure 4 *PLCδ1* silencing impairs $[Ca^{2+}]_i$ elevation and NFAT activation. (**a**) NHEK treated with either non- (control; filled diamond) or *PLCδ1*-targeting (siPLCδ1#1, open triangle; siPLCδ1#2, open circle) siRNAs were loaded with Fura-2-AM. $[Ca^{2+}]_i$ was measured in recording medium without adding $CaCl_2$, and then upon addition of 2 mM $CaCl_2$. Results are representative of three trials. (**b**) NHEK treated with either non- (control; filled diamonds) or *PLCδ1*-targeting (siPLCδ1; open circles) siRNAs were loaded with Fura-2-AM. The cells were then treated with thapsigargin (TG; to deplete intracellular calcium stores) in recording medium without adding $CaCl_2$ and then in the presence of 2 mM $CaCl_2$ (to induce Ca^{2+} entry). Results are representative of three trials. (**c**) NHEK treated with either non- (control) or *PLCδ1*-targeting (siPLCδ1#1 and siPLCδ1#2) siRNAs were stained for NFATc4 after 48 h of incubation in medium containing 1.2 mM $CaCl_2$. Scale bar = 100 μm. Images are representative of four trials. (**d**) NFAT transcriptional activity in NHEK treated with either non- (control) or *PLCδ1*-targeting (siPLCδ1#1 and siPLCδ1#2) siRNAs and grown in medium with (high Ca^{2+}) or without (low Ca^{2+}) 1.2 mM $CaCl_2$ was measured by a luciferase assay. Data are represented as mean ± S.E.M. ($N = 3$ in each group). (**e**) Lucifer yellow fluorescence was visualized in sections of human organotypic skin cultures. Either vehicle or an NFAT inhibitor (11R-VIVIT) was added to the medium in the last 72 h. Nuclei were counter-stained with Hoechst (blue). Dotted lines denote the skin culture surface. Scale bar = 30 μm. Images are representative of three trials. Stained sections were assessed in a blinded fashion by two independent observers. Statistical significance was assessed using Welch's *t*-test. $^{**}P < 0.01$

Table 2 TEER of NHEK treated with either vehicle (0 μM) or an NFAT inhibitor

11 R-VIVIT	0 μM	12.5 μM	25 μM
TEER ($\Omega\ cm^2$)	210 ± 7.9	150 ± 2.7**	87 ± 3.7**

$^{**}P < 0.01$ versus 0 μM
Mean ± S.E.M. ($N = 3$ in each group). Welch's *t*-test

Figure S9a). In addition, discontinuous staining of ZO-1 was observed in some parts of 11R-VIVIT-treated organotypic skin culture (Supplementary Figure S9b). Furthermore, the lucifer yellow penetration assay showed lucifer yellow accumulation in the upper SC of the 11R-VIVIT-treated skin culture (Figure 4e), indicating that the SC barrier is affected. These results suggest that the impaired NFAT signal contributes to the defective epidermal barrier.

PLCδ1 downregulation impairs skin barrier through hyperactivation of p38 MAPK. Activation of MAPKs is a critical event in the terminal differentiation of keratinocytes and in barrier integrity maintenance.[25] Immunoblotting revealed that PLCδ1 knockdown increased phosphorylated-p38 MAPK in NHEK under undifferentiated (low $CaCl_2$) and differentiated (high $CaCl_2$) conditions (Figure 5a). In contrast to p38 MAPK, PLCδ1 knockdown did not alter the amount of phosphorylated ERK (Supplementary Figure S10a). General stress and toxic stimuli are known to activate p38 MAPK.[26]

However, *PLCδ1* silencing did not affect stress- or toxicity-induced cellular responses such as ATP release (Figure 5b) or expression of ER stress markers (Supplementary Figure S10b), suggesting that the hyperactivation of p38 MAPK is not due to general stress or toxic stimuli. Interestingly, pharmacological inhibition of NFAT activated p38 MAPK (Figure 5c), suggesting that defective NFAT activation hyperactivates p38 MAPK in PLCδ1-knocked down NHEK. We further confirmed that phosphorylated-p38 MAPK was increased in the PLCδ1-knocked down human organotypic skin culture (Figure 5d) and epidermis of PLCδ1 cKO mice (Figures 5e and f). Then, we examined whether p38 MAPK hyperactivation contributes to RhoA inhibition and defective TJ formation in PLCδ1-knocked down NHEK. Treatment of NHEK with SB202190, a p38 MAPK inhibitor, decreased the phosphorylated form of HSP27, a downstream effector of p38 MAPK (Figure 5g). This indicates that SB202190 treatment effectively inhibits p38 MAPK activity in PLCδ1-knocked down NHEK. In the presence of SB202190, PLCδ1 downregulation did not affect RhoA-GTP levels (Figure 5h), implying that hyperactivated p38 MAPK inhibits RhoA in PLCδ1-knocked down NHEK. We further examined the effect of p38 MAPK inhibition on defective TJ formation in PLCδ1-knocked down NHEK. SB202190 treatment restored ZO-1 membrane localization (Figure 5i) and increased TEER (Table 1) in PLCδ1-knocked down NHEK without affecting the amount of TJ proteins such as ZO-1 and claudin-1 (Supplementary Figure S9c), suggesting that aberrantly activated p38 MAPK is involved in defective TJ formation. As activation of p38 MAPK induces expression of inflammatory cytokines,[27] hyperactivation of p38 MAPK may disturb TJ formation through secretion of inflammatory cytokines in PLCδ1-knocked down NHEK. To test this possibility, we transferred medium from *PLCδ1*-silenced NHEK to normal NHEK. Although PLCδ1 knockdown induces mRNA expression of inflammatory cytokines, likely through p38 MAPK hyperactivation (Supplementary Figure S11a), conditioned medium from *PLCδ1*-silenced NHEK did not alter localization of ZO-1 and TEER (Supplementary Figure S11b; Supplementary Table S2), suggesting that PLCδ1 downregulation does not induce secretion of a sufficient amount of cytokines to affect formation and function of TJ. Inhibition of p38 MAPK also restored normal expression of filaggrin and active caspase-14 in PLCδ1-knocked down organotypic skin culture (Supplementary Figure S5c). In addition, topical application of p38 MAPK inhibitor on PLCδ1 cKO skin restored normal expression of ZO-1 (Figure 5j). SC thickness looked normal with p38 MAPK inhibitor (Figure 5j). Furthermore, inhibition of p38 MAPK restored the barrier permeability in PLCδ1-knocked down human organotypic skin culture (Figure 5k), implying that hyperactivated p38 MAPK contributes to SC barrier defects.

Hyperactivation of p38 MAPK is involved in the pathogenesis of psoriasis-like skin inflammation. As PLCδ1 protein is downregulated in IMQ-induced psoriasis-like inflammation in mice,[13] we examined the activation status of p38 MAPK in the skin of IMQ-induced psoriasis-like inflammation. Immunoblotting and immunohistochemistry revealed that phosphorylated-p38 MAPK was increased in the skin and epidermis of IMQ-treated mice (Figures 6a and b). Concomitant with PLCδ1 downregulation (Supplementary Figure S12),[13] phosphorylated-p38 MAPK was also increased in the epidermis of patients with psoriasis (Figure 6c). In addition, ZO-1 mislocalization was observed in parakeratotic SC in the epidermis of patients with psoriasis, where PLCδ1 was downregulated (Supplementary Figure S12). We next examined the effects of SB202190 treatment on the expression of barrier defect- and psoriasis-related genes in IMQ-induced psoriasis-like inflammation. The expression of S100A8 is induced by barrier disruption.[28] Real-time RT-PCR revealed that SB202190 treatment decreased S100A8 expression (Figure 6d). In addition, SB202190 treatment reduced the expression of the key pathogenic cytokines in psoriasis (Figure 6d) and attenuated IMQ-induced ear swelling (Figure 6e). These results strongly suggest that hyperactivation of p38 MAPK, presumably downstream of PLCδ1 downregulation, contributes to barrier defects and the pathogenesis of psoriasis-like skin inflammation in mice.

Discussion

A defective epidermal barrier is a feature of psoriasis.[5] Although PLCδ1 is downregulated in the lesional skin of patients with psoriasis,[13] whether PLCδ1 downregulation affects the epidermal barrier was not known. Our results show that PLCδ1 downregulation in keratinocytes impairs skin barrier integrity in gene-modified mice, human organotypic skin culture, and NHEK. We also showed that dysregulation of $[Ca^{2+}]_i$, NFAT, p38 MAPK, and RhoA contribute to the skin barrier defects caused by PLCδ1 downregulation. On the basis of these results, we propose a hypothetical mechanism for the barrier defects by PLCδ1 downregulation (Figure 6f). In this model, PLCδ1 downregulation impairs $[Ca^{2+}]_i$ elevation and NFAT activation in keratinocytes. Then, p38 MAPK is aberrantly activated, leading to RhoA inhibition. Without sufficient RhoA activity, TJ proteins are mislocalized, leading to impaired formation of the SC barrier. Finally, these barrier defects contribute to the aggravation of psoriasis-like inflammation.

PLCδ1 downregulation disturbed the localization of the TJ proteins. Interestingly, altered localization of TJ proteins is observed in both fully developed psoriasis plaques[29] and early-stage psoriasis,[30] suggesting that abnormal localization of TJ proteins is involved in the pathogenesis and aggravation of psoriasis. Although ZO-1 mislocalization was observed in lesional skin of patients with psoriasis, the pattern of ZO-1 mislocalization was different from that of PLCδ1 cKO mice and PLCδ1-knocked down organotypic skin cultures. Besides PLCδ1 downregulation-mediated mislocalization of ZO-1, it is possible that inflammatory cytokines-mediated SC malformation could contribute to aberrantly broad ZO-1 staining in parakeratotic SC in psoriasis. PLCδ1 is abundantly expressed in the SG. As proper TJ formation in the SG is crucial for proper SC barrier function,[31,32] PLCδ1 may impair SC barrier through abnormal TJ formation. Despite mislocalization of ZO-1 and occludin, PLCδ1 KO mice did not increase transepidermal water loss. In addition, PLCδ1 downregulation did not abolish TJ barrier against biotin tracer in organotypic skin culture.

Other TJ components may compensate for mislocalization of ZO-1 and occludin, and loss of PLCδ1 may induce only subtle TJ dysfunctions *in vivo*. Interestingly, despite of mislocalization of TJ proteins, TJ dysfunction was not observed in lesional skin of psoriasis.[33] It is possible that subtle TJ dysfunction disturbed ion concentrations and the liquid environment at the SG-SC interface, leading to abnormal SC formation in PLCδ1 cKO skin and lesional skin of psoriasis. Given that mislocalization of TJ proteins itself affects terminal differentiation of keratinocytes and SC formation,[34] it is also possible that PLCδ1 downregulation affects SC formation not by impairing TJ functions but by disturbing localizatiuon of TJ proteins.

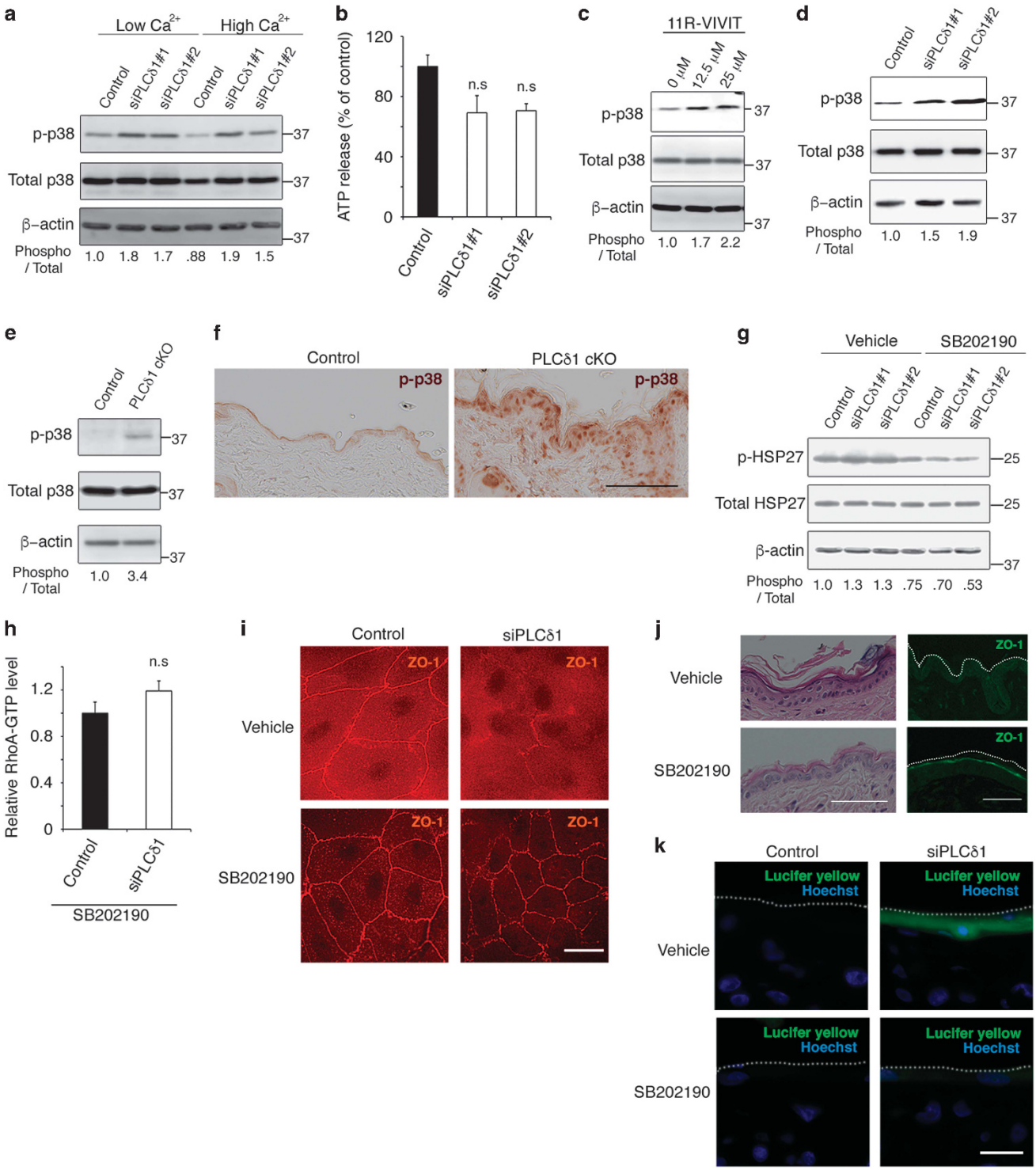

Proinflammatory cytokines affect SC barrier integrity. As abnormalities of SC barrier were observed at the same time as the onset of skin inflammation in PLCδ1 cKO mice, we cannot rule out the possibility that the loss of PLCδ1 impaired the SC barrier through induction of proinflammatory cytokines *in vivo*. We showed that PLCδ1 downregulation disturbs barrier integrity through inflammatory immune cell-independent mechanisms in organotypic skin cultures and that conditioned medium from PLCδ1-knocked down NHEK did not induce TJ defects in NHEK. Given these observations, PLCδ1 downregulation appears to directly impair the SC and TJ barrier, at least in an *in vitro* system.

SC barrier disruption by tape stripping induces the production of pathogenic cytokines associated with psoriasis, including IL-17 and IL-23.[35] We previously reported that IL-17 and IL-23 are upregulated in PLCδ1 cKO skin.[13] Given that PLCδ1 cKO mice show SC barrier defects, these defects might cause upregulation of these psoriasis-related cytokines in PLCδ1 cKO skin.

Interestingly, treatment with psoriasis-related cytokines decreased PLCδ1 mRNA expression in NHEK (Supplementary Figure S13a). As psoriasis-related cytokines are induced by SC barrier disruption,[35] it is possible that PLCδ1 is downregulated in the epidermis of patients with psoriasis as a consequence of SC barrier defects. Indeed, barrier disruption by tape stripping decreased PLCδ1 expression in mouse skin (Supplementary Figure S13b). Given these observations, there might be a vicious cycle of PLCδ1 downregulation, SC barrier defects, and cytokine overproduction in psoriatic skin (Supplementary Figure S13c).

A defective SC barrier is also a characteristic of AD. However, PLCδ1 cKO mice did not present the major features of AD, such as overproduction of Th2 cytokines and heightened itching. Barrier disruption by PLCδ1 downregulation might not be sufficient for induction of the AD-like immune responses characterized by Th2 skewing. Nonetheless, understanding the molecular mechanisms underlying epidermal barrier formation might help identify new therapeutic targets in barrier-defective skin diseases such as psoriasis and AD. This study identified PLCδ1 as a critical player for epidermal barrier integrity and suggests that PLCδ1 and its downstream molecules might be useful therapeutic targets.

Materials and Methods

Mice. *PLCδ1*$^{-/-}$ (PLCδ1 KO) mice, *K14-Cre*$^{+}$*PLCδ1*$^{fl/fl}$ keratinocyte-specific PLCδ1 KO (cKO) mice, and *Foxn1::PLCδ1*$^{+}$*PLCδ1*$^{-/-}$ (Tg/KO) mice were generated as described previously.[13,36] IL-17A/F double KO mice were also generated as described previously.[37] PLCδ1 KO and IL-17A/F double KO mice were crossed to generate IL-17A/F, PLCδ1 triple KO mice. We used *PLCδ1*$^{+/-}$ and *K14-Cre*$^{+}$*PLCδ1*$^{fl/+}$ mice as controls for *PLCδ1*$^{-/-}$ and *K14-Cre*$^{+}$*PLCδ1*$^{fl/fl}$ mice, respectively, as PLCδ1$^{+/-}$ mice and *K14-Cre*$^{+}$*PLCδ1*$^{fl/+}$ mice did not show any phenotypic differences from their wild-type counterparts.[13] Age-matched littermates were used to minimize any effects of genetic background. Therefore, potential genetic modifiers of phenotypes would be randomly distributed among the experimental and control groups. Female BALB/c mice were purchased from Tokyo Laboratory Animals Science (Tokyo, Japan). Mice aged 8–10 weeks were used to induce psoriasis-like skin inflammation by IMQ. Ears were pretreated with 40 μl of 20 μM SB202190 (Wako, Osaka, Japan) or vehicle (acetone) and then treated daily with a topical dose of 12.5 mg of commercially available IMQ cream (5%) (Beselna Cream; Mochida Pharmaceuticals, Tokyo, Japan) for 4 days. Ear swelling was measured with a dial thickness gauge (Peacock, Tokyo, Japan). *K14-Cre*$^{+}$*PLCδ1*$^{fl/fl}$ mice were treated on their shaved back skin with 40 μl of 20 μM SB202190 or vehicle (acetone) daily for four days. Transepidermal water loss was measured on shaved back skin with a Tewameter TW300 (Courage Khazaka Electronics, Cologne, Germany). All animal studies were approved by the animal experiments review board of Tokyo University of Pharmacy and Life Sciences.

RNA extraction and real-time RT-PCR. Total RNA was isolated using the RNeasy Mini kit (Qiagen, Hilden, Germany) or the Reliaprep RNA Cell Miniprep System (Promega, Madison, WI, USA), according to the manufacturers' protocols. Complementary DNA was synthesized from total RNA using the ReverTra Ace qPCR RT kit (Toyobo, Osaka, Japan). Real-time PCR was performed using the THUNDERBIRD SYBR qPCR Mix (Toyobo) in a CFX96 thermocycler (Bio-Rad, München, Germany). The relative amounts of target gene mRNAs were normalized to glyceraldehyde 3-phosphate dehydrogenase (GAPDH) mRNA.

Dye exclusion assay. Outside–inside barrier function was evaluated by examining FITC (Sigma-Aldrich, St. Louis, MO, USA) penetration into the epidermis as described previously.[38] Briefly, shaved dorsal skin was treated with 100 μl of 0.05% FITC diluted in acetone and dibutyl phthalate (1:1). Three hours later, the treated area was tape-stripped nine times to remove the FITC in the upper SC. The treated area (1.2 cm × 1.2 cm) was removed, and the epidermis was separated from the dermis by soaking the skin in phosphate-buffered saline (PBS) at 60 °C for

Figure 5 *PLCδ1* silencing activates p38 MAPK. (**a**) Immunoblotting of phosphorylated (p-p38) and total p38 MAPK in NHEK treated with either non- (control) or *PLCδ1*-targeting (siPLCδ1#1 and siPLCδ1#2) siRNAs, and grown in medium either with (high Ca^{2+}) or without (low Ca^{2+}) 1.2 mM $CaCl_2$. β-actin was used as a loading control. Results are representative of two trials. (**b**) Extracellular ATP concentrations were measured in conditioned medium of NHEK treated with either non- (control) or *PLCδ1*-targeting (siPLCδ1#1 and siPLCδ1#2) siRNAs. ($N = 4$ in each group). (**c**) Immunoblotting of phosphorylated (p-p38) and total p38 MAPK in the presence of an NFAT inhibitor (11 R-VIVIT; treated for 24 h with the concentrations indicated). β-actin was used as a loading control. Results are representative of two trials. (**d**, **e**) Immunoblotting of phosphorylated (p-p38) and total p38 MAPK in human organotypic skin cultures treated with either non- (control) or *PLCδ1*-targeting (siPLCδ1#1 and siPLCδ1#2) siRNAs (**d**) and the epidermis of control and keratinocyte-specific PLCδ1 knockout (cKO) mice (**e**). β-actin was used as a loading control. Results are representative of two trials (**d**) or three animals per group (**e**). (**f**) Skin from control and PLCδ1 cKO mice were stained with an antibody against phosphorylated-p38 MAPK (brown). Scale bar = 50 μm. Images are representative of three animals per group. Stained sections were assessed in a blinded fashion by two independent observers. (**g**) Immunoblotting of phosphorylated (p-HSP27) and total HSP27 in NHEK treated with either non- (control) or *PLCδ1*-targeting (siPLCδ1#1 and siPLCδ1#2) siRNAs, and either vehicle or a p38 MAPK inhibitor (SB202190). β-actin was used as a loading control. Results are representative of two trials. (**h**) NHEK treated with either non- (control) or *PLCδ1*-targeting (siPLCδ1#1 and siPLCδ1#2) siRNAs were pretreated with either vehicle or SB202190, and then exposed to 2 mM $CaCl_2$ for 15 min. RhoA-GTP levels were determined using G-LISA in NHEK stimulated with Ca^{2+}. RhoA-GTP levels were normalized to the total protein amount. Data are represented as mean ± S.E.M. ($N = 3$ in each group). (**i**) Immunofluorescence detection of ZO-1 in NHEK treated with either non- (control) or *PLCδ1*-targeting siRNAs, grown in medium containing 1.2 mM $CaCl_2$ for 24 h in the presence of either vehicle or SB202190. Scale bar = 50 μm. Images are representative of three trials. (**j**) Skin samples of control and keratinocyte-specific PLCδ1 knockout (cKO) mice treated with either vehicle or SB202190, and were stained with H&E or an antibody against ZO-1. Dotted lines denote the skin surface. Scale bar = 50 μm (H&E), and 20 μm (ZO-1). Images are representative of five animals per group. (**k**) Lucifer yellow fluorescence was visualized in sections of human organotypic skin cultures treated with either non- (control) or *PLCδ1*-targeting (PLCδ1siRNA) siRNAs. Either vehicle or SB202190 was added to the medium in the last 72 h of culture. Nuclei were counter-stained with Hoechst (blue). Dotted lines denote the skin culture surface. Scale bar = 30 μm. Images are representative of three trials. Stained sections were assessed in a blinded fashion by two independent observers. (**a**, **c**, **d**, **e** and **g**) Relative ratios of phosphorylated to total protein (Phospho/Total) are denoted below each panel. Statistical significance was assessed using Welch's *t*-test. n.s; not significant

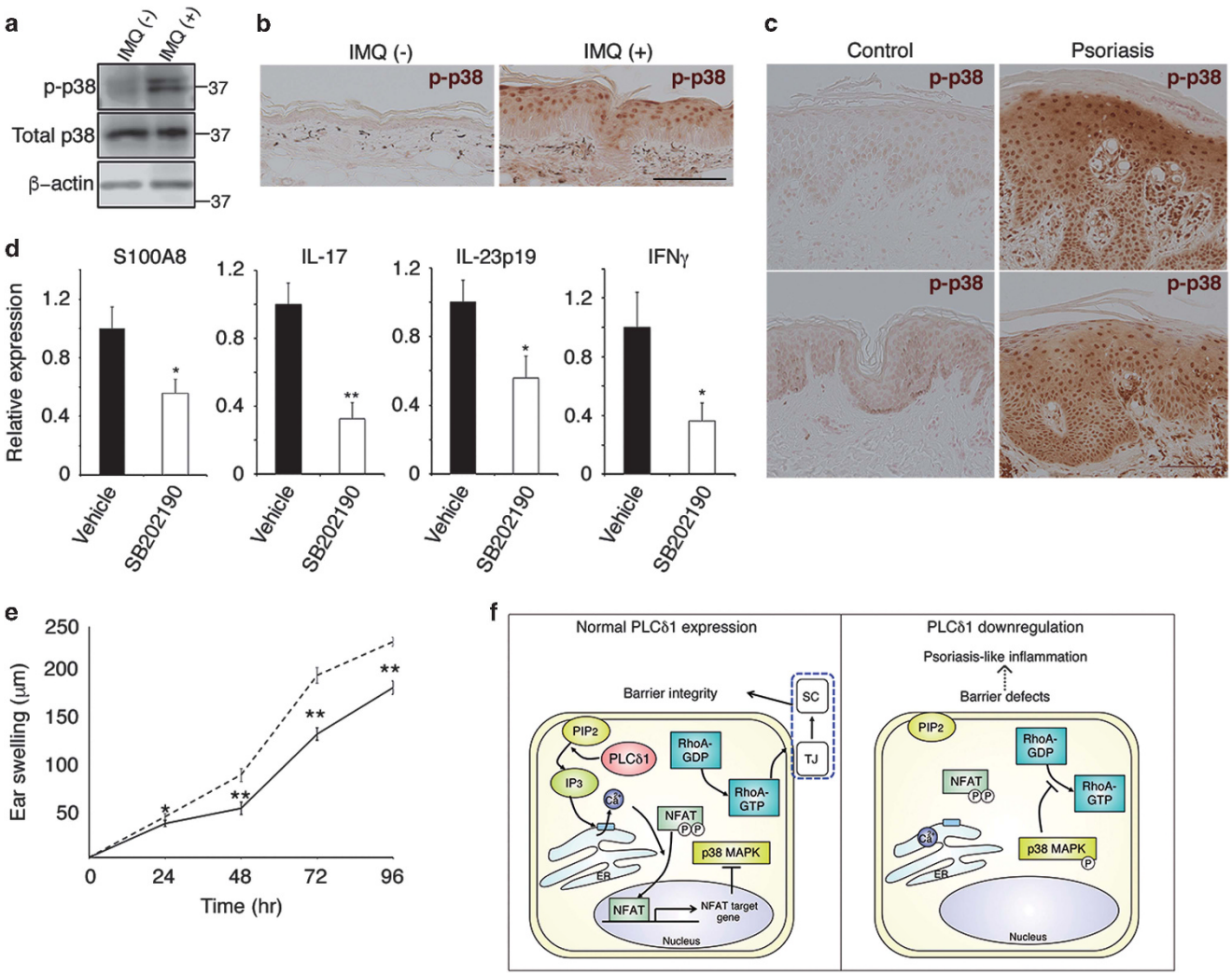

Figure 6 Hyperactivation of p38 MAPK is involved in psoriasis-like skin inflammation. (**a**) Immunoblotting of phosphorylated (p-p38) and total p38 MAPK in the epidermis of imiquimod-treated (IMQ (+)) and untreated (IMQ (−)) mice. β-actin was used as a loading control. Results are representative of four animals per group. (**b**) Skin from IMQ (−) and IMQ (+) mice were stained with an antibody against phosphorylated-p38 MAPK (brown). Scale bar = 50 μm. Images are representative of four animals per group. Stained sections are assessed in a blinded fashion by two independent observers. (**c**) Skin from non-psoriasis volunteers (control) and patients with psoriasis (psoriasis) were stained with an antibody against phosphorylated-p38 MAPK (brown). Scale bar = 50 μm. Images are representative of five non-psoriasis volunteers and six patients with psoriasis. Stained sections were assessed in a blinded fashion by two independent observers. (**d**) S100A8, IL-17A, IL-23p19, and interferonγ (IFNγ) mRNA expression in dorsal skin of imiquimod-treated mice treated with either vehicle or SB202190 was determined by real-time RT-PCR. All values were normalized to GAPDH. Results are displayed as arbitrary units (expression in vehicle-treated skin (vehicle) = 1). Data are represented as the mean ± S.E.M. (N = 6 in each group). (**e**) Time course of ear swelling in mice treated with either vehicle (dotted line) or SB202190 (solid line) after imiquimod treatment. Ear swelling was measured at the indicated times. Data are mean ± S.E.M. (N = 6 in each group). (**f**) Hypothetical model of the PLCδ1 regulatory mechanisms for barrier integrity. In the keratinocytes of the SG, PIP_2 is hydrolyzed to IP_3 by PLCδ1, leading to Ca^{2+} release from intracellular Ca^{2+} stores and $[Ca^{2+}]_i$ elevation. $[Ca^{2+}]_i$ elevation induces dephosphorylation of NFAT, leading to its nuclear translocation and induction of NFAT target genes. NFAT activation prevents aberrant activation of p38 MAPK through by unknown mechanisms. Thus, RhoA is thus activated, leading to the formation of TJ. Upon proper TJ formation, a normal SC is also formed, which maintains barrier integrity. Without sufficient PLCδ1 (right panel), PIP_2 is not hydrolyzed and IP_3-mediated Ca^{2+} release and subsequent NFAT activation are inhibited. Without active NFAT, p38 MAPK is hyperactivated, leading to RhoA inhibition and defective TJ and SC formation. This p38 MAPK hyperactivation-mediated barrier defects contribute to the pathogenesis of psoriasis. Statistical significance was assessed using Welch's t-test. $^*P<0.05$, $^{**}P<0.01$

1 min. The epidermis was then homogenized in PBS and fluorescence intensity measured at 460 nm with a SH-9000 microplate reader (Corona Electric, Ibaraki, Japan). Frozen sections were also prepared from skin samples after tape stripping. FITC accumulation in the epidermis was analyzed using a BZ-8000 microscope (Keyence, Osaka, Japan). For toluidine blue staining, mice were sacrificed and dehydrated by sequential incubation in 25, 50, 75, and 100% methanol. After rehydration in PBS, they were incubated for 1 min in 0.1% toluidine blue (Sigma-Aldrich) and destained with PBS. Lucifer yellow permeability assays were performed with P8 mice as described previously.[39] Briefly, the mice were euthanized and immersed for 1 h at 37 °C in 1 mM lucifer yellow (Sigma-Aldrich) dissolved in PBS. Ventral skin was collected and frozen sections were prepared. These sections were fixed in 4% paraformaldehyde and counter-stained using Hoechst dye. Sections were observed under a BZ-X700 microscope (Keyence).

Histology. Skin was fixed overnight in 4% paraformaldehyde and embedded in paraffin. After deparaffinization and rehydration, skin sections were stained using either toluidine blue or Congo Red (Sigma-Aldrich). Sections were then examined under a BX51 microscope (Olympus, Tokyo, Japan). Nile red staining was performed on frozen sections, which were examined under a BZ-8000 microscope (Keyence).

Transmission electron microscopy. Skin was fixed with a 2% paraformaldehyde, 2% glutaraldehyde solution in 0.1 M cacodylate buffer (pH 7.4), followed by postfixation with 2% osmium tetroxide in 0.1 M cacodylate buffer. Then, skin was dehydrated through a series of graded ethanol solutions, infiltrated with propylene oxide (PO), and put into a 70:30 mixture of PO and resin (Quetol-812; Nisshin EM, Tokyo, Japan). Next, the skin was embedded in the resin. The blocks were ultra-thin sectioned at 70 nm and stained with 2% uranyl acetate, followed by secondary staining with lead stain solution (Sigma-Aldrich). The samples were observed under a JEM-1200EX (JEOL, Tokyo, Japan).

CEs preparation. A defined area of dorsal mouse skin (25 mm^2) was boiled in isolation buffer [20 mM Tris-HCl, pH 7.5; 5 mM EDTA; 10 mM dithiothreitol (DTT); and 2% sodium dodecyl sulfate (SDS)] with vigorous shaking for 40 min. After centrifugation, the CEs were washed twice with isolation buffer and were analyzed using a hemocytometer. For sonication experiments, the CEs suspension was sonicated and intact CEs were counted with a hemocytometer.

***In situ* transglutaminase activity assay.** *In situ* transglutaminase activity assay was performed as reported previously.[40] In brief, cryosections were blocked with 1% BSA in 0.1 M Tris-HCl pH 8.4 for 30 min and then incubated for 1 h at room temperature with 50 μM Alexa-Fluor-594–cadaverine (Life Technologies, Carlsbad, CA, USA) in 0.1 M Tris-HCl pH 8.4 containing Hoechst and 5 mM $CaCl_2$. The reaction was stopped by incubating the sections with 25 mM EDTA in PBS for 5 min. Sections were observed under a BZ-X700 microscope (Keyence).

Enzyme-linked immunosorbent assay. Serum IgE and IgG_1 levels were determined using the Quantikine Mouse IgE and IgG_1 Immunoassay kits (R&D Systems, Minneapolis, MN, USA), respectively, according to the manufacturer's instructions.

Cell culture. NHEK (KURABO, Osaka, Japan) were cultured in HuMedia-KG2 (KURABO) supplemented with insulin, bovine pituitary extract, epidermal growth factor, hydrocortisone, kanamycin, and amphotericin B. Cells from third passage were used for the experiments. Both non-targeting and human *PLCδ1*-targeting siRNA duplexes were synthesized by Hokkaido System Science (Sapporo, Japan). The human *PLCδ1*-targeting sequences were as follows: 5′-CGUUAGGAAUAAC ACUGCA-3′ (siPLCδ1#1) and 5′-GCUUCUUGGUGGAAGAUUA-3′ (siPLCδ1#2). The sequence of the non-targeting siRNA was 5′-UUCUCCGAACGUGUCACGU-3′. The siRNAs were introduced into NHEK with Lipofectamine RNAiMax (Life Technologies). After 72 h of incubation, the cells were collected. To induce differentiation, 1.2 mM $CaCl_2$ was added to the culture medium for the last 24 h of incubation.

Organotypic skin culture and lucifer yellow permeability assay. NHEK were seeded onto cell culture inserts (Millipore, Billerica, MA, USA) containing collagen gel and human dermal fibroblasts 24 h after siRNA transfection and cultured overnight in assay medium (Japan Tissue Engineering, Aichi, Japan). Next, the cultures were raised to the air-liquid interface and cultured in assay medium for 6 days to form a multilayered epidermis. Either 20 μM SB202190 or 11 R-VIVIT (25 μM; Millipore) was added to the assay medium for the last 48 or 72 h of culture. The lucifer yellow permeability assay was performed as described previously.[41] Briefly, 20 μl of 1 mM lucifer yellow was added to the surface of the organotypic skin cultures and incubated for 2 h. Frozen sections of the organotypic skin cultures were prepared and lucifer yellow permeability was assessed under a BZ-8000 or BZ-X700 microscope (Keyence).

Analysis of skin permeability using biotin tracers. Organotypic skin cultures were either placed on a 20 μl drop of 2 mg/ml LZ-Link Sulfo-NHS-LC-Biotin (Thermo Scientific, Rockford, IL, USA) and incubated for 30 min. Frozen sections of the organotypic skin cultures were prepared and biotin was labeled with streptavidin conjugated to Alexa 594 (Life Technologies) to visualize biotin. The slides were assessed under a BZ-X700 microscope (Keyence).

Human subjects. Patients with psoriasis and volunteers without psoriasis were enrolled. Informed consent was obtained from all participants. The study protocol was approved by the Ethics Committee of Kyoto University and was conducted in accordance with the Declaration of Helsinki Principles.

Immunofluorescence and immunohistochemistry. For immunofluorescence with NHEK, the cells were fixed in 4% paraformaldehyde, permeabilized with 0.1% Triton X-100, and blocked with 0.5% bovine serum albumin (BSA). Next, the cells were incubated with anti-ZO-1 (Life Technologies), anti-claudin-1 (Abcam, Cambridge, UK), anti-occludin (Life Technologies), anti-E-cadherin (BD Biosciences, San Jose, CA, USA), and anti-NFATc4 (Santa Cruz Biotechnology, Santa Cruz, CA, USA) antibodies. Binding was detected by subsequent incubation of the cells with an Alexa-Fluor 488 or 568-conjugated secondary antibody. Counter-staining was performed with Hoechst 33258 (Life Technologies). For immunofluorescence detection of active caspase-14,[42] occludin, ZO-1, K1 (Covance, Emeriville, CA, USA), K5 (Covance), loricrin (Covance), involucrin (NeoMarkers, Fremont, CA, USA), filaggrin (Novocastra, Newcastle, UK), and Ki67 (Novocastra), frozen sections of organotypic skin cultures and mouse skin were prepared. These sections were fixed in 4% paraformaldehyde, blocked with 0.5% BSA, and then incubated with the primary and secondary antibodies. Immunohistochemistry of phosphorylated-p38 MAPK (Cell Signaling Technology, Danver, MA, USA), claudin-1, and PLCδ1 (Sigma-Aldrich) was carried out on paraffin sections, according to the manufacturer's instructions. Sections were observed under a BZ-8000 or BZ-X700 microscope (Keyence).

TEER measurement. NHEK were seeded on cell culture inserts (Millipore) 24 h after siRNA transfection, and grown until confluent. The medium was then replaced with high Ca^{2+} medium containing 1.2 mM $CaCl_2$. After 48 h of incubation, TEER was measured using a Millicell-ERS (Millipore).

RhoA and Rac1 activation assay. RhoA activity was assessed by a GST-RBD pull-down assay in NHEK. Purification of GST-RBD and pull-down assays for active RhoA were performed as described previously.[43] The G-LISA assay for RhoA and Rac1 was performed with Colorimetric G-LISA activity assay kits (Cytoskeleton, Denver, CO, USA) according to the manufacturer's protocol for quantitative assessment of GTP-bound RhoA and Rac1 levels in NHEK.

ATP release. ATP levels in NHEK conditioned medium were measured by the luciferin-based ENLITEN ATP Assay (Promega) according to the manufacturer's instructions.

Ca^{2+} imaging. NHEK were loaded with 5 μM Fura-2 AM in recording medium [20 mM HEPES (pH 7.4), 115 mM NaCl, 5.4 mM KCl, 0.8 mM $MgCl_2$, 7.5 mM glucose]. Fluorescence (ratio of F340 nm to F380 nm) from single cells was acquired at 37 °C with an inverted microscope (IX-71; Olympus) equipped with a cooled CCD camera (Orca-II-ER; Hamamatsu Photonics, Shizuoka, Japan), a filter exchanger, and appropriate filters controlled by the TI Workbench software developed by T. Inoue (Japan). The signals from more than 30 single cells for each preparation were recorded and an average profile was calculated.

Luciferase assay. Luciferase assays using the pNFAT-Luc plasmid were performed as described previously.[36] Briefly, 24 h after siRNA transfection, the reporter constructs were introduced into NHEK. Twenty-four hours after transfection, the medium was replaced with high Ca^{2+} medium containing 1.2 mM $CaCl_2$. Then, 24 h after medium replacement, luciferase activity was measured, using the Dual-Luciferase Reporter Assay System (Promega).

Conditioned medium from PLCδ1-silenced NHEK. Conditioned medium was prepared by incubating control or PLCδ1-knocked down NHEK in HuMedia-KG2 (KURABO) supplemented with insulin, bovine pituitary extract, epidermal growth factor, hydrocortisone, kanamycin, amphotericin B, and 1.2 mM $CaCl_2$ for 24 h. Then, conditioned medium from control or PLCδ1-knocked down NHEK was added to NHEK and NHEK were cultured for 24 h.

Statistical analysis. Results are expressed as mean $\pm$ S.E.M. Statistical analyses were achieved with at least three samples in each group using a two-sided Welch's *t*-test, which corrects for biases due to an unequal number of samples or variances between the different groups.

Conflict of Interest

The authors declare no conflict of interest.

Acknowledgements. We thank Drs T Hibino, M Miyai and M Yamamoto-Tanaka for providing the active caspase-14-specific antibody and technical assistance. We also thank Drs M Murakami and K Yamamoto for technical assistance in transepidermal water loss measurements. This work was supported by the Uehara Memorial Foundation, a Grant-in-Aid for Scientific Research (B), and AMED-CREST to KF, as well as a Grant-in-Aid for Scientific Research (C), Ono Medical Research Foundation, the Kowa Life Science Foundation, the Naito Foundation, and PRIME to YN.

1. Candi E, Schmidt R, Melino G. The cornified envelope: a model of cell death in the skin. *Nat Rev Mol Cell Biol* 2005; **6**: 328–340.
2. Lippens S, Denecker G, Ovaere P, Vandenabeele P, Declercq W. Death penalty for keratinocytes: apoptosis versus cornification. *Cell Death Differ* 2005; **12**: 1497–1508.
3. Palmer CN, Irvine AD, Terron-Kwiatkowski A, Zhao Y, Liao H, Lee SP *et al.* Common loss-of-function variants of the epidermal barrier protein filaggrin are a major predisposing factor for atopic dermatitis. *Nat Genet* 2006; **38**: 441–446.
4. Irvine AD, McLean WH, Leung DY. Filaggrin mutations associated with skin and allergic diseases. *N Engl J Med* 2011; **365**: 1315–1327.
5. Roberson ED, Bowcock AM. Psoriasis genetics: breaking the barrier. *Trends Genet* 2010; **26**: 415–423.
6. Segre JA. Epidermal barrier formation and recovery in skin disorders. *J Clin Invest* 2006; **116**: 1150–1158.
7. de Cid R, Riveira-Munoz E, Zeeuwen PL, Robarge J, Liao W, Dannhauser EN *et al.* Deletion of the late cornified envelope LCE3B and LCE3C genes as a susceptibility factor for psoriasis. *Nat Genet* 2009; **41**: 211–215.
8. Bergboer JG, Oostveen AM, de Jager ME, den Heijer M, Joosten I, van de Kerkhof PC *et al.* Paediatric-onset psoriasis is associated with ERAP1 and IL23R loci, LCE3C_LCE3B deletion and HLA-C*06. *Br J Dermatol* 2012; **167**: 922–925.
9. Bikle DD, Xie Z, Tu CL. Calcium regulation of keratinocyte differentiation. *Expert Rev Endocrinol Metab* 2012; **7**: 461–472.
10. Naeem AS, Zhu Y, Di WL, Marmiroli S, O'Shaughnessy RF. AKT1-mediated Lamin A/C degradation is required for nuclear degradation and normal epidermal terminal differentiation. *Cell Death Differ* 2015; **22**: 2123–2132.
11. Xie Z, Chang SM, Pennypacker SD, Liao EY, Bikle DD. Phosphatidylinositol-4-phosphate 5-kinase 1alpha mediates extracellular calcium-induced keratinocyte differentiation. *Mol Biol Cell* 2009; **20**: 1695–1704.
12. Calautti E, Li J, Saoncella S, Brissette JL, Goetinck PF. Phosphoinositide 3-kinase signaling to Akt promotes keratinocyte differentiation versus death. *J Biol Chem* 2005; **280**: 32856–32865.
13. Kanemaru K, Nakamura Y, Sato K, Kojima R, Takahashi S, Yamaguchi M *et al.* Epidermal phospholipase Cδ1 regulates granulocyte counts and systemic interleukin-17 levels in mice. *Nat Commun* 2012; **3**: 963.
14. Downing DT. Lipid and protein structures in the permeability barrier of mammalian epidermis. *J Lipid Res* 1992; **33**: 301–313.
15. Gutowska-Owsiak D, Schaupp AL, Salimi M, Selvakumar TA, McPherson T, Taylor S *et al.* IL-17 downregulates filaggrin and affects keratinocyte expression of genes associated with cellular adhesion. *Exp Dermatol* 2012; **21**: 104–110.
16. Gutowska-Owsiak D, Ogg GS. Cytokine regulation of the epidermal barrier. *Clin Exp Allergy* 2013; **43**: 586–598.
17. Howell MD, Kim BE, Gao P, Grant AV, Boguniewicz M, Debenedetto A *et al.* Cytokine modulation of atopic dermatitis filaggrin skin expression. *J Allergy Clin Immunol* 2007; **120**: 150–155.
18. Ichinohe M, Nakamura Y, Sai K, Nakahara M, Yamaguchi H, Fukami K. Lack of phospholipase C-delta1 induces skin inflammation. *Biochem Biophys Res Commun* 2007; **356**: 912–918.
19. Hoste E, Kemperman P, Devos M, Denecker G, Kezic S, Yau N *et al.* Caspase-14 is required for filaggrin degradation to natural moisturizing factors in the skin. *J Invest Dermatol* 2011; **131**: 2233–2241.
20. Denecker G, Hoste E, Gilbert B, Hochepied T, Ovaere P, Lippens S *et al.* Caspase-14 protects against epidermal UVB photodamage and water loss. *Nat Cell Biol* 2007; **9**: 666–674.
21. Jackson B, Peyrollier K, Pedersen E, Basse A, Karlsson R, Wang Z *et al.* RhoA is dispensable for skin development, but crucial for contraction and directed migration of keratinocytes. *Mol Biol Cell* 2011; **22**: 593–605.
22. Al-Daraji WI, Grant KR, Ryan K, Saxton A, Reynolds NJ. Localization of calcineurin/NFAT in human skin and psoriasis and inhibition of calcineurin/NFAT activation in human keratinocytes by cyclosporin A. *J Invest Dermatol* 2002; **118**: 779–788.
23. Santini MP, Talora C, Seki T, Bolgan L, Dotto GP. Cross talk among calcineurin, Sp1/Sp3, and NFAT in control of p21(WAF1/CIP1) expression in keratinocyte differentiation. *Proc Natl Acad Sci USA* 2001; **98**: 9575–9580.
24. Crabtree GR, Olson EN. NFAT signaling: choreographing the social lives of cells. *Cell* 2002; **109**: S67–S79.
25. Eckert R, Efimova T, Dashti SR, Balasubramanian S, Deucher A, Crish JF *et al.* Keratinocyte survival, differentiation, and death: many roads lead to mitogen-activated protein kinase. *J Invest Dermatol* 2002; **7**: 36–40.
26. Roux PP, Bleins J. ERK and p38 MAPK-activated protein kinases: a family of protein kinases with diverse biological functions. *Microbiol Mol Biol Rev* 2004; **2**: 320–344.
27. Zarubin T, Han J. Activation and signaling of the p38 MAP kinase pathway. *Cell Res.* 2005; **15**: 11–18.
28. Eckert RL, Broome AM, Ruse M, Robinson N, Ryan D, Lee K. S100 proteins in the epidermis. *J Invest Dermatol* 2004; **123**: 23–33.
29. Pummi K, Malminen M, Aho H, Karvonen SL, Peltonen J, Peltonen S. Epidermal tight junctions: ZO-1 and occludin are expressed in mature, developing, and affected skin and in vitro differentiating keratinocytes. *J Invest Dermatol* 2001; **117**: 1050–1058.
30. Kirschner N, Poetzl C, von den Driesch P, Wladykowski E, Moll I, Behne MJ *et al.* Alteration of tight junction proteins is an early event in psoriasis: putative involvement of proinflammatory cytokines. *Am J Pathol* 2009; **175**: 1095–1106.
31. Sugawara T, Iwamoto N, Akashi M, Kojima T, Hisatsune J, Sugai M *et al.* Tight junction dysfunction in the stratum granulosum leads to aberrant stratum corneum barrier function in claudin-1-deficient mice. *J Dermatol Sci* 2013; **70**: 12–18.
32. Yuki T, Komiya A, Kusaka A, Kuze T, Sugiyama Y, Inoue S. Impaired tight junctions obstruct stratum corneum formation by altering polar lipid and profilaggrin processing. *J Dermatol Sci* 2013; **69**: 148–158.
33. Kirschner N, Houdek P, Fromm M, Moll I, Brandner JM. Tight junctions form a barrier in human epidermis. *Eur J Cell Biol* 2010; **89**: 839–842.
34. Kirschner N, Brandner JM. Barriers and more: functions of tight junction proteins in the skin. *Ann N Y Acad Sci* 2012; **1257**: 158–166.
35. Gregorio J, Meller S, Conrad C, Di Nardo A, Homey B, Lauerma A *et al.* Plasmacytoid dendritic cells sense skin injury and promote wound healing through type I interferons. *J Exp Med* 2010; **207**: 2921–2930.
36. Nakamura Y, Fukami K, Yu H, Takenaka K, Kataoka Y, Shirakata Y *et al.* Phospholipase Cdelta1 is required for skin stem cell lineage commitment. *EMBO J* 2003; **22**: 2981–2991.
37. Ishigame H, Kakuta S, Nagai T, Kadoki M, Nambu A, Komiyama Y *et al.* Differential roles of interleukin-17 A and -17 F in host defense against mucoepithelial bacterial infection and allergic responses. *Immunity* 2009; **30**: 108–119.
38. Moniaga CS, Egawa G, Kawasaki H, Hara-Chikuma M, Honda T, Tanizaki H *et al.* Flaky tail mouse denotes human atopic dermatitis in the steady state and by topical application with *Dermatophagoides pteronyssinus* extract. *Am J Pathol* 2010; **176**: 2385–2393.
39. Augustin I, Gross J, Baumann D, Korn C, Kerr G, Grigoryan T *et al.* Loss of epidermal Evi/Wls results in a phenotype resembling psoriasiform dermatitis. *J Exp Med* 2013; **210**: 1761–1777.
40. Leclerc EA, Huchenq, Kezic S, Serre G, Jonca N. Mice deficient for the epidermal dermokine β and γ isoforms display transient cornification defects. *J Cell Sci* 2014; **127**: 2862–2872.
41. Mildner M, Jin J, Eckhart L, Kezic S, Gruber F, Barresi C *et al.* Knockdown of filaggrin impairs diffusion barrier function and increases UV sensitivity in a human skin model. *J Invest Dermatol* 2010; **130**: 2286–2294.
42. Hibino T, Fujita E, Tsuji Y, Nakanishi J, Iwaki H, Katagiri C *et al.* Purification and characterization of active caspase-14 from human epidermis and development of the cleavage site-directed antibody. *J Cell Biochem* 2010; **109**: 487–497.
43. Ren XD, Schwartz MA. Determination of GTP loading on rho. *Methods Enzymol* 2000; **325**: 264–272.

Supplementary Information accompanies this paper on *Cell Death and Differentiation* website (http://www.nature.com/cdd)